

Forward Deformation of PET Volumes Using Non-Uniform Elastic Material Constraints

Gregory J. Klein

Lawrence Berkeley National Laboratory, Berkeley, CA 94720, USA**
GJKlein@lbl.gov

Abstract. A method for non-rigidly deforming 3D PET datasets is described. The method uses a Lagrangian motion field description and a forward deformation mapping. To regularize the deformation, an anisotropic strain energy function is used that separately models the material properties of cardiac and background tissues. The method is applied to motion compensation in PET so that different time frames of a cardiac sequence may be combined.

1 Introduction

In gated acquisition of cardiac Positron Emission Tomography (PET), motion of the heart is stopped in the images by dividing the data obtained during each cardiac cycle into a number of different time frames, or gates. An unfortunate effect of distributing the data into many time frames is that the statistical quality of each reconstructed volume suffers, and the individual images appear very noisy. Ideally, one would like to correct the images for cardiac motion, then add them back together to obtain a composite image with less motion blur and better contrast to noise properties.

We describe here a deformable motion technique that allows motion compensation for subsequent combination of PET datasets. A source volume representing the heart at end systole will be deformed to match a reference volume representing the heart at end diastole. The deformed source will then be summed with the reference to produce a composite volume with better contrast to noise characteristics. Though a gated cardiac study typically results in some 10 - 15 gates, each representing a short portion of the cardiac cycle, this paper will just focus on the combination of two time frames. Unique in the approach are two aspects. First, a non-uniform regularization constraint incorporating anisotropic strain energy is used to model the underlying cardiac tissue. Second, a forward deformation mapping is used which insures that each voxel in a source dataset contributes to the calculation of a deformed volume. The work is most closely related to 3D deformable motion work based on optical flow algorithms [1, 2] and material elastic models [3, 4].

** Supported by NIH grant HL25840 and DOE contract DE-AC03-76SF00098

2 Motion Estimation

As is the case with most 3D deformable algorithms, this algorithm is based on two general criteria. An image matching constraint first attempts to find a motion field that warps a source volume to best match a reference volume. Because numerous image matching transformations exist which equally satisfy the image matching constraint, the solution is regularized by imposing an additional criterion constraining motion field smoothness. This latter requirement treats the volume as a continuously stretching and bending medium that can only deform as is consistent with elastic material models. In our smoothness constraint formulation, we use a pre-segmented volume which masks the heart. This enables smoothing of the motion field to be carried out differently in cardiac tissue than is done in the adjacent tissue and blood pool.

The motion estimation framework is described as follows. Define two 3D density fields, a source volume, $f_1(\mathbf{r})$, and a reference volume, $f_2(\mathbf{r})$, where $\mathbf{r} = (x, y, z)$ represents the voxel index. A dense Lagrangian motion field is defined as $\mathbf{m}(x, y, z) = (u(x, y, z), v(x, y, z), w(x, y, z))$ and the deformed volume of f_1 is defined as $\hat{f}(\mathbf{r}) = f_1(\mathbf{r} + \mathbf{m})$. With these definitions, we can express an image matching error term, $e_I(\mathbf{r})$, and an anisotropic material strain energy term [5], $e_S(\mathbf{r})$, at each voxel location \mathbf{r} , as follows:

$$e_I(\mathbf{r}) = \gamma_I(f_2(\mathbf{r}) - \hat{f}(\mathbf{r}))^2 \quad (1)$$

and

$$e_S(\mathbf{r}) = \frac{\lambda}{2}(u_x + v_y + w_z)^2 + \mu(u_x^2 + v_y^2 + w_z^2) + \frac{\mu}{2}(u_y^2 + u_z^2 + v_x^2 + v_z^2 + w_x^2 + w_y^2 + 2u_yv_x + 2u_zw_x + 2v_zw_y) \quad (2)$$

where γ_I is a global scalar used to alter the balance between the two error terms, λ and μ are elasticity terms called the Lamé constants, and where derivatives of the motion field are denoted as $u_x = du/dx$.

It can be seen that the λ term in equation (2) penalizes non-zero divergence and the μ term penalizes sharp discontinuities in the motion field. For highly incompressible fields, the Poisson ratio, $\nu = \lambda/(2(\lambda + \mu))$, approaches a maximum of 0.5, which yields a divergence term, λ , that approaches infinity. The Lamé constants used in equation (2) are global constants for isotropic materials. Obviously, the elastic properties of the myocardium are drastically different from the blood pool inside the ventricle, and from the adjacent lung tissue and air space. In this formulation, we implement an anisotropic elastic model by using a segmented voxel mask to delineate voxels representing cardiac tissue, and represent λ and μ by vector fields instead of just two global scalars. The vector fields for each term take on two values, one value in the region labeled cardiac tissue, and another value in the background regions. As such, separate elastic properties can be ascribed to cardiac tissue and to adjacent regions. We assume here that a technique is available to obtain a reasonably correct segmentation

of the cardiac tissue from the background, though it is noted that this may not always be a trivial task, and may itself be a formidable research question in some cases.

Though the motion field describing the volume deformation is a one-to-one mapping in a continuous domain, implementation on a discrete domain involves some subtleties that are important to recognize in the deformation of PET datasets. Past efforts [2–4] have used a reverse transformation to calculate voxel values in the deformed volume. In this Eulerian formulation, the motion vectors describe a particle’s motion with respect to its final position. To obtain the value of each voxel in the deformed volume, $\hat{f}(\mathbf{r}) = f_1(\mathbf{r} - \mathbf{m})$, eight voxels from the deformation volume are sampled at the location, $\mathbf{r} - \mathbf{m}$, and weighted according to trilinear interpolation. Such *backward* sampling does not guarantee that each voxel in the source volume will contribute to the deformed volume. We use a Lagrangian forward sampling technique which distributes each voxel value of the source volume using normalized Gaussian weighting in a single-pass calculation of the deformation. Though the forward sampling scheme does not guarantee absolute conservation of total voxel intensities, it does guarantee that every voxel in the source volume contributes to the deformation volume. Also, the normalized Gaussian weighting of the displaced voxels prevents artifacts in the non-uniformly sampled deformation.

The overall minimization problem is to find a motion field consistent with elastic material properties that best matches the deformed volume to the reference volume via a minimization of:

$$E_{tot} = \sum_{\mathbf{r}} [e_I(\mathbf{r}) + e_S(\mathbf{r})] \quad (3)$$

We invoke a minimization technique similar to the approach proposed by Zhou [2], which linearizes the calculation of an optimal deformed volume by using a Taylor series approximation. Assuming the true motion field is \mathbf{m} , and the current estimate is $\tilde{\mathbf{m}}$, then a Taylor series approximation of $\hat{f}(\mathbf{r})$ can be expressed in terms of a delta motion field, $(\delta u, \delta v, \delta w) = \delta \mathbf{m} = \tilde{\mathbf{m}} - \mathbf{m}$, as $\hat{f}(\mathbf{r}) = f_1(\mathbf{r} + \tilde{\mathbf{m}}) - \nabla f_1(\mathbf{r} + \tilde{\mathbf{m}})\delta \mathbf{m}$. Substituting the expression, $\tilde{\mathbf{m}} - \delta \mathbf{m}$, for \mathbf{m} in the constraint equations results a quadratic functional in $\delta \mathbf{m}$ that can be minimized via the calculus of variations [6]. The resulting Euler-Lagrange equations are solved using finite differencing techniques and a conjugate gradient method. At each step, $\hat{f}(\mathbf{r})$ is calculated and the conjugate gradient algorithm is used to find the best $\delta \mathbf{m}$ satisfying the equations. This delta motion field is added to the current total motion field and the procedure is repeated. For the results presented in this paper, ten to fifteen iterations of this outer loop were typically required to reach an overall solution. Each conjugate gradient step usually converges quickly, and also requires some ten to twenty iterations.

3 Results

Two cardiac phantoms were used to test the algorithm. The first is a simple model of gated emission PET consisting of a ellipsoidal building blocks forming

the human torso [7]. The second is a finite element model (FEM) based on a parametric prolate spheroid description of a left ventricle which has been fitted to MRI data acquired from a canine heart [8]. Included in the model is the incompressible nature of cardiac tissue and non-symmetric cardiac muscle fiber orientation.

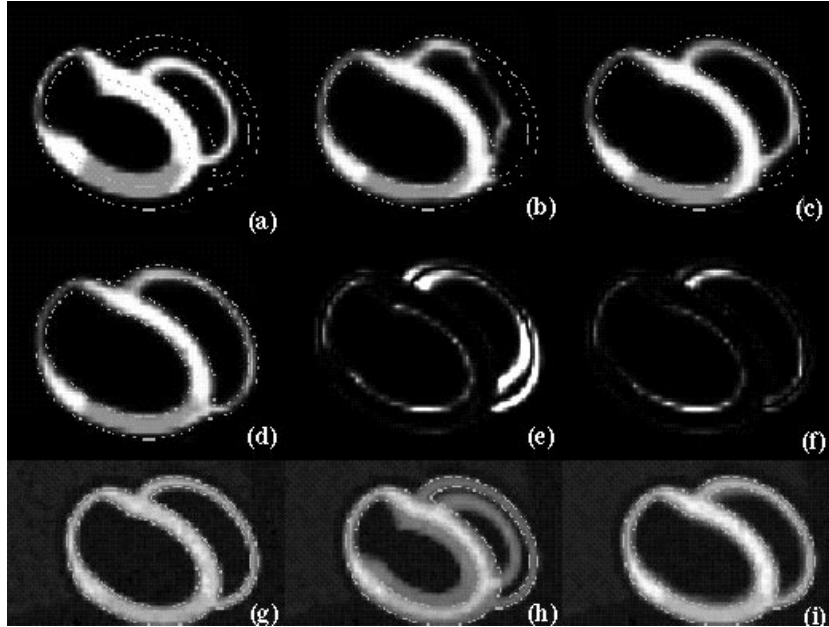


Fig. 1. Ellipsoidal phantom results

Fig. 1 shows the results on the simple model. The source volume representing end systole is seen in (a). The reference volume representing end diastole is seen as an edge map overlaid on (a). An attempt at deforming the source volume using an isotropic strain energy function penalizing non-zero divergence (Poisson ratio = 0.46) shows in (b) that the non-zero divergence in the blood pool makes it difficult for the algorithm to find the correct deformation. Relaxing the divergence penalty allows a better match, seen in (c). However, the best match is obtained using an anisotropic strain energy function penalizing non-zero divergence and smoothness only in the cardiac tissue (d). Mean squared error (MSE) values between the reference volume and cases (b), (c) and (d) are 1727, 1234 and 555 respectively. Image difference maps between the reference and cases (c) and (d) are shown in (e) and (f). These further demonstrate that the anisotropic strain energy function produces the warped volume best matching the reference. It is noted that in order to find a suitable deformation in case (c), the image weighting term needed to be double the value that was used for the anisotropic

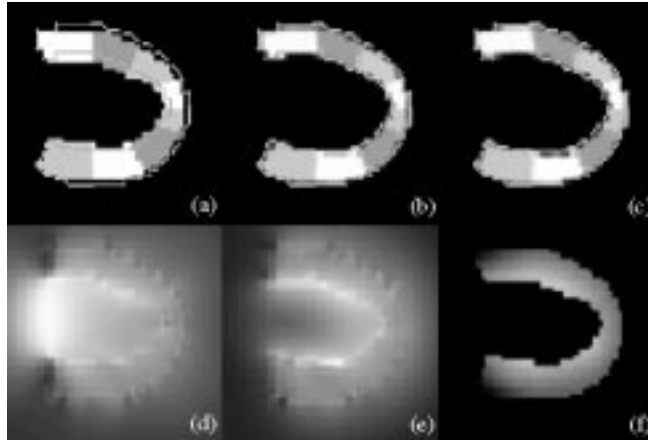


Fig. 2. Parametric FEM results

case. This is troublesome, since one would not like to weight the image matching criteria so much that physically implausible motions are estimated.

As a display of the utility of this algorithm, (g), (h) and (i) show a comparison of noisy versions of the phantom summed with and without motion compensation. Obviously, if no motion compensation is done, as seen in (h), then blur due to the motion is induced which severely obscures image features. By first deforming the systole volume to match the heart shape at end diastole, and then summing (i), the contrast to noise ratio is improved over the reference volume alone (g). This is the desired result which allows us to combine gated PET datasets and increase image quantification without loss of resolution.

Results using the FEM are seen in Fig. 2. A 16 element model was used to determine the shape of the left ventricle as it was passively inflated. Here the inflated state is used as a reference volume, and the deflated state is the source volume. Because a parametric description of the two states is available, the "ground truth" motion vectors may be calculated which bring any two points into correspondence. The source volume and an edge map of the reference are seen in (a). To better visualize performance of the deformation algorithm, texture was added to the model by giving each of the 16 elements a slightly different voxel value. Deformed volumes using isotropic strain (b) and anisotropic strain (c) look similar; both match the reference fairly well. MSE values with respect to the reference are 1117 and 1002 respectively, so the anisotropic model performs only slightly better with respect to this measure. Comparing motion field magnitudes of the isotropic (d) and anisotropic (e) results versus the true motion field magnitude (f) reveals that the anisotropic model is considerably more accurate with respect to this measure. MSE values of the true magnitude volume (f) compared to (d) and (e) are 36661 and 17481 respectively. The motion magnitude images point out how the isotropic strain model falters in the region where image divergence is present (in the blood pool). Since there was a zero

background in this case, the motion field error in the background region does not induce much error in the deformed volume for the isotropic case. This would not be true in general for real PET data where voxel intensities in the blood pool would be small, yet not negligible.

4 Concluding Remarks

When deforming a volume to match a reference dataset, there is always a balance between the weight of the image matching constraints and the regularization constraints. Because numerous motion fields can produce identical deformed images, it is the function of the regularization constraints to prevent physically unrealizable motion fields. In the deformation of real PET datasets, where considerable statistical noise is present, there is always the danger of weighting the image matching terms too greatly so that uncorrelated "hot spots" in the datasets are matched even though they do not originate from the same segment of cardiac tissue. The motivation for this work was to incorporate a more realistic, nonuniform elastic model into the regularization constraint so that this term could be weighted more heavily, and thus would prevent solutions with physically implausible motion fields. Though the technique required a prior segmentation step, because the segmentation was only used during the regularization process, and not during the final image warping calculation, the algorithm should not be sensitive to minor segmentation errors. The improvements shown in this paper by the anisotropic model over the isotropic strain model indicate that this more realistic model can be worth the added expense of the requirement for a segmented cardiac volume.

References

1. S. M. Song, R. M. Leahy, D. P. Boyd, B. H. Brundage, and S. Napel. Determining cardiac velocity fields and intraventricular pressure distribution from a sequence of Ultrafast CT cardiac images. *IEEE Trans. Med Imag*, **13** (1994) 386–397.
2. Z. Zhou, C. E. Synolakis, R. M. Leahy, and S. M. Song. Calculation of 3D internal displacement fields from 3D X-ray computer tomographic images. *Proc. R. Soc. Lond. A*, **449** (1937) 537–555, 1995.
3. R. Bajcsy, R. Kovacic. Multiresolution elastic matching. *Comput. Vision, Graph., Image Proc.*, 46:1-21, 1989.
4. G. E. Christensen, R. D. Rabbitt, and M. I. Miller. 3d brain mapping using a deformable neuroanatomy. *Phys Med Biol*, 39:609-618, 1994.
5. K. Washizu. *Variational Methods in Elasticity and Plasticity*. Pergamon Press, Oxford, 1982.
6. B. K. P. Horn. *Robot Vision*. The MIT Press, Cambridge, Massachusetts, 1986.
7. J. A. Terry, B. M. W. Tsui, J. R. Perry, and G. T. Gullberg. A three-dimensional mathematical phantom of the human torso for use in SPECT imaging research studies. *J Nucl Med*, 31(5):868, 1990.
8. K. D. Costa, P. J. Hunter, J. S. Wayne, L. K. Waldman, J. M. Guccione, and A. D. McCulloch. A three-dimensional finite element method for large elastic deformations of ventricular myocardium: II - prolate spheroidal coordinates. *Trans. ASME*, 118:464-472, 1996.